Geochemistry Geophysics Geosystems G3

Article
Volume 13, Number 11
29 November 2012
Q11014, doi:10.1029/2012GC004435
ISSN: 1525-2027

Published by AGU and the Geochemical Society

The Zagros core: Deformation of the continental lithospheric mantle

Keith Priestley, Dan McKenzie, and Jamie Barron
Bullard Laboratories, University of Cambridge, Madingley Rise, Cambridge CB3 0EZ, UK (kfp10@cam.ac.uk)

Mohammad Tatar
International Institute of Earthquake Engineering and Seismology, Tehran 19537, Iran

Eric Debayle
Laboratoire de Géologie de Lyon: Terre, Planètes et Environnement, Université de Lyon 1 and Ecole Normale Supérieure de Lyon, FR-67622 Villeurbanne, France

[1] The Zagros of Iran form one of the youngest collisional orogenic belts on Earth. At shallow depths, shortening across the Zagros is accommodated by folding in the sediments, high-angle thrust faulting in the basement and thickening of the lower crust, but how shortening is accommodated by the lithospheric mantle has been uncertain largely because the upper mantle seismic structure has been poorly known. We map the lateral variations in upper mantle shear wave speed beneath this region using a large, multi-mode surface wave data set. The upper mantle is slow for most of the Middle East, but a high shear wave speed lid extending to ∼225 km depth exists beneath the Zagros. We use a $T(V_s, z)$ relation to convert the shear wave speed profiles to temperature profiles and fit these with geotherms to identify the base of the lithosphere. The upper mantle temperatures from the seismic model are consistent with temperatures derived from geochemical modeling. The lithosphere is less than ∼120 km thick over the region except for a thick lithospheric root beneath the Zagros, implying that shortening in the mantle is accommodated by lithospheric thickening. The composition of the volcanic rocks from above the area of the thickened lithosphere has depleted magma source regions with densities ∼60 kg m^{-3} less than the MORB source. Elsewhere in the Middle East the volcanic source regions have compositions and densities similar to that of MORB. The shortening across the Zagros is accommodated by lithospheric thickening but the cool thickened lithosphere has been stabilized from delamination by depletion.

Components: 6600 words, 8 figures.

Keywords: lithosphere; surface wave; tomography.

Index Terms: 7219 Seismology: Seismic monitoring and test-ban treaty verification; 7270 Seismology: Tomography (6982, 8180); 8120 Tectonophysics: Dynamics of lithosphere and mantle: general (1213).

Received 19 September 2012; **Revised** 17 October 2012; **Accepted** 18 October 2012; **Published** 29 November 2012.

Priestley, K., D. McKenzie, J. Barron, M. Tatar, and E. Debayle (2012), The Zagros core: Deformation of the continental lithospheric mantle, *Geochem. Geophys. Geosyst.*, *13*, Q11014, doi:10.1029/2012GC004435.

1. Introduction

[2] A collision between continents can produce spectacular surficial geology, as is now seen in the Himalaya Mountains and the Tibetan Plateau. The shortening that occurs during continental collision results in crustal roots beneath both the mountains and plateaus, but how the mantle portion of the lithosphere accommodates the convergence is a contentious topic. If thickened lithospheric mantle consists of cool, undepleted material, its negative buoyancy with respect to the surrounding mantle could result in it delaminating and sinking into the deeper mantle [*Bird*, 1978; *Houseman et al.*, 1981]. On the other hand, if the thickened lithospheric mantle comprises depleted material [*Jordan*, 1975], delamination may be inhibited even though the thickened lithosphere is cool with respect to the surrounding asthenosphere. The Himalaya-Tibet orogen is the best-studied example of continent-continent collision. The Indo-Eurasia collision initiated about 55 Ma and is now well advanced.

[3] The Arabian-Eurasian collision, which has produced the East Anatolian and Iranian Plateaus, is younger and may provide clues to our understanding of the earlier stages of the continent-continent collision process. The East Anatolian and Iranian Plateaus (Figure 1) form a broad zone of deformation located between the relatively rigid Arabian and Eurasian plates. Starting in the Late Cretaceous the landmass that now forms the plateaus was assembled by the accretion of island arcs and other continental fragments to the southern margin of Eurasia [e.g., *Şengör*, 1990; *Şengör et al.*, 2008]. The Arabian plate was part of the Nubian Shield until 30–35 Ma when it rifted from Africa [*Martinez and Cochran*, 1988]. The collision between Arabia and Eurasia began in the early Miocene (~16–23 Ma) [*Robertson*, 2000] and was preceded by the subduction of the oceanic lithosphere of the Neo-Tethys beneath eastern Turkey and Iran. The subsequent northward motion of the Arabian plate following the final closure of the Neo-Tethys Ocean about 12 Ma [*Dewey et al.*, 1986; *McQuarrie et al.*, 2003] has given rise to the East Anatolian and Iranian Plateaus north and east of the Bitlis-Zagros suture, respectively (Figure 1). The convergence of Arabia with Eurasia is accommodated by the westward extrusion of the Anatolian Block along the North and East Anatolian faults and by shortening within the East Anatolian and Iranian Plateaus.

[4] During the Eocene (34–56 Ma), subduction of the Neo-Tethys beneath Eurasia built a large subduction-accretion complex in the region of the present-day East Anatolian Plateau [*Şengör et al.*, 2003, 2008]. The last marine sediments in eastern Anatolia were deposited ~12 Ma [*Gelati*, 1975] and uplift of the plateau commenced soon afterwards [*Şengör et al.*, 2003, 2008]. The earliest volcanism following the closure of the Neo-Tethys Ocean occurred about 11 Ma, became widespread by 6–8 Ma and has continued to the present, but the type of volcanism has changed over time from calc-alkaline to alkaline [*Pearce et al.*, 1990]. The region now has an average elevation of more than 2 km and more than half of the plateau is covered with young volcanics, in some places exceeding 1 km in thickness [*Keskin*, 2003]. *McQuarrie et al.* [2003] suggest that the Arabia-Eurasia convergence has been relatively constant at a rate of 2–3 cm/yr for the past 59 Ma, a value similar to GPS-derived rates [e.g., *McClusky et al.*, 2003; *Reilinger et al.*, 2006]. Crustal seismicity is widespread, but no subcrustal earthquakes have been located [*Turkelli et al.*, 2003].

[5] The Zagros Mountains, the active fold-and-thrust belt along the eastern portion of the Zagros-Bitlis suture on the leading edge of the Arabian plate, forms the southwestern boundary of the Iranian Plateau. The Zagros consist of long, linear folds which form a 200–300 km-wide series of ranges extending ~1500 km from eastern Turkey to the Strait of Hormuz (Figure 1). The high level of seismicity observed in the Zagros shows that the belt continues to be active, but the lack of subcrustal seismicity [e.g., *Maggi et al.*, 2000b; *Tatar et al.*, 2004] indicates that subduction has ceased. Within Iran about half of the present-day Arabian-Eurasian convergence (~10 mm/yr) is accommodated by shortening in the Zagros Mountains [*Tatar et al.*, 2002] and is accomplished by a combination of folding in the sediments [*Sattarzadeh et al.*, 1999], high-angle thrust faulting in the basement [*Jackson*, 1980; *McQuarrie*, 2004], and thickening of the lower crust [*Hatzfeld et al.*, 2003; *Paul et al.*, 2006]. The remainder of the Arabian-Eurasian convergence at the longitude of Iran is accommodated across the Alborz Mountains, the Kopet Dagh Mountains and the South Caspian Basin [*Vernant et al.*, 2004]. The South Caspian Basin, probably of oceanic origin, is now being overthrust by the Alborz from the south and the Talesh Mountains from the west [*Priestley et al.*, 1994; *Jackson et al.*, 2002; *Tatar et al.*, 2007].

[6] *Ni and Barazangi* [1986] suggest that the Zagros are a young analogue of the Himalaya. Both result from continent–continent collision, but the

10.1029/2012GC004435

India-Eurasia convergence is faster, the Himalaya are at a more mature stage and their structure is better understood. In comparison, the crust and upper mantle structure and the processes forming the East Anatolian and Iranian Plateaus are still poorly known; it is unclear as to how the shortening in the mantle of the Iranian Plateau, in particular, has been accommodated. Various authors [e.g., *Molinaro et al.*, 2005; *Hafkenscheid et al.*, 2006; *Agard et al.*, 2011] have suggested that the mantle portion of the

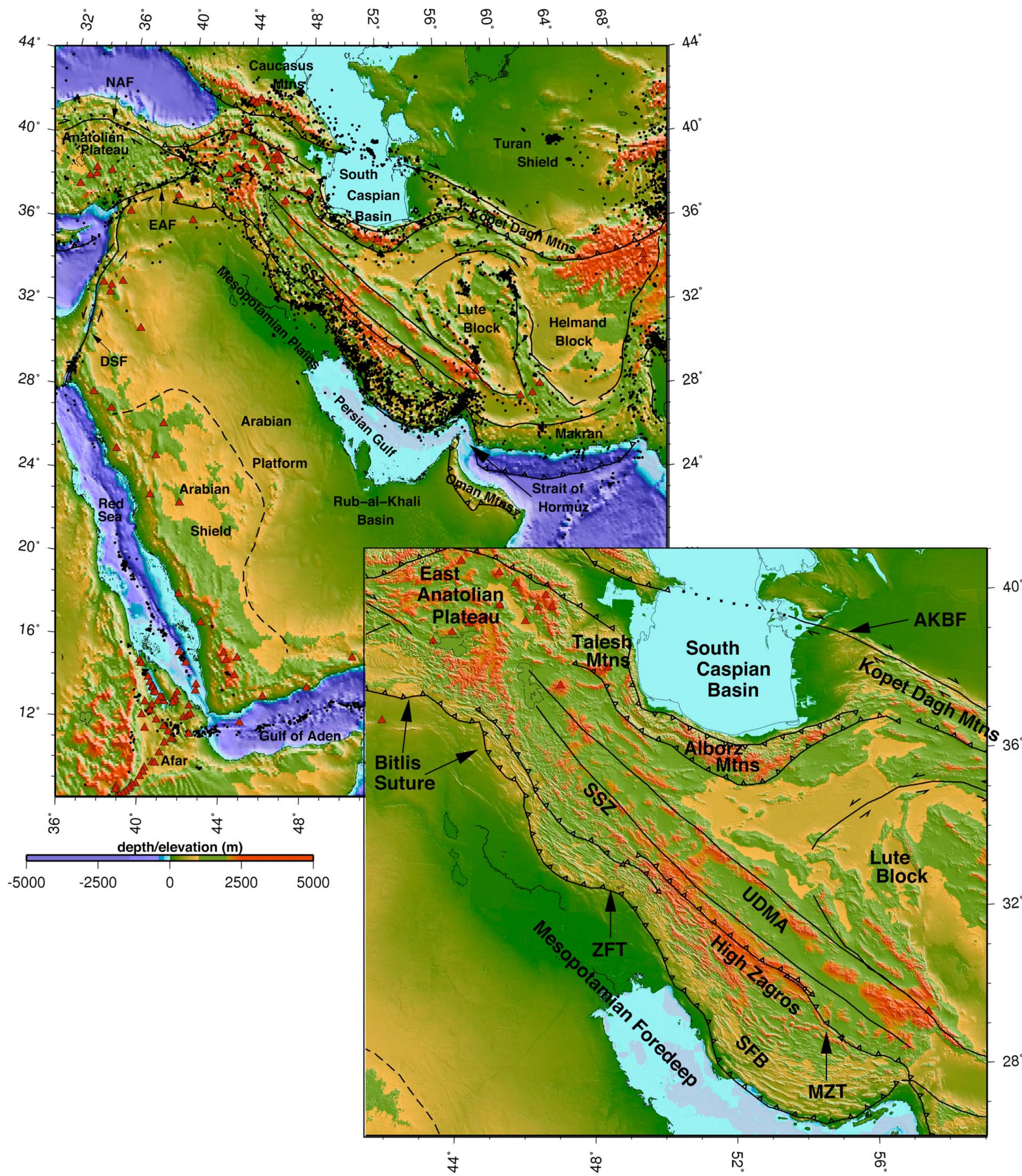

Figure 1

lithosphere has foundered, but there is little seismic evidence to corroborate this.

[7] In this paper we use primarily surface wave tomography to examine the upper mantle structure of the region; we show the existence of a thickened, high-velocity upper mantle beneath the Mesopotamian Foredeep and the Zagros Mountains but no evidence for a high-velocity upper mantle to the northeast beneath central Iran or to the northwest beneath the East Anatolian Plateau. We propose that this feature beneath the Mesopotamian Foredeep and the Zagros Mountains is a high-velocity keel resulting from the shortening of the lithospheric mantle.

2. Upper Mantle Shear Wave Structure of the Middle East

2.1. Surface Wave Data and Analysis

[8] We analyze the waveforms of earthquakes listed in the CMT catalog that occurred between 1977 and 2010 in the region including and surrounding the Middle East (Figure 2a). We analyze publicly available seismograms from IRIS, Geoscope and GEOFON permanent stations, temporary PASSCAL seismic deployments from IRIS and data from the broadband seismic networks within Iran operated by the International Institute for Earthquake Engineering and Seismology (IIEES) in Tehran and the University of Mashad. In addition, we have incorporated data from temporary seismic networks installed by IIEES, the Institute for Advanced Studies in Basic Sciences (IASBS) in Zanjan, the Laboratoire de Géophysique Interne et de Tectonophysique (LGIT) in Grenoble, France, and the University of Cambridge (UCam) (Figure 2b). These data provide excellent fundamental and higher-mode (Figure 2c) path coverage for the region (Figures 2e–2j) by using a large number of relatively short propagation paths (Figure 2d).

[9] Our analysis method is summarized in *Cara and Lévêque* [1987], *Debayle* [1999], *Debayle and Kennett* [2000], *Debayle and Sambridge* [2004] and *Maggi et al.* [2006]. In brief, our tomographic model is derived by first inverting the individual surface waveforms in the 50–160 s period range for a path-average S_v-model using the automated version [*Debayle*, 1999] of the *Cara and Lévêque* [1987] technique. An important advantage of this method is that higher-mode information can be retrieved from seismograms recorded over relatively short paths, giving additional information to that of the fundamental-mode constraints on the shallow upper mantle structure and providing greater sensitivity compared to the fundamental mode in the deeper upper mantle. Each inverted waveform results in a path-average S_v-wave speed model ($V_{S_v}(z)$) and an *a posteriori* error ($\sigma_D(z)$). The *a posteriori* error accounts only for errors in the waveform fit and not systematic errors such as those associated with the event's focal parameters. Since many of the propagation paths are similar, we cluster measurements for paths with epicenters within a 2° cap recorded at stations within a 2° cap. For each cluster, we determine the mean shear wave velocity at each depth and its error ($\sigma_M(z)$) which is significantly larger than $\sigma_D(z)$. Many of the clusters consist of a small number of paths and $\sigma_M(z)$ may be underestimated. For these clusters, we assume the errors to be similar to the $\sigma_M(z)$

Figure 1. Tectonic maps of the Middle East and the main elements of the Zagros orogen. Red triangles denote locations of Quaternary volcanoes; black dots denote epicenters of magnitude 5 and greater earthquakes from *Engdahl et al.* [1998] and its updates. The enlarged map at lower right shows details of the Zagros orogen. From southwest to northeast the Zagros orogen can be divided into five divisions – the foreland basin, the Simply Folded Belt (SFB), the High Zagros or Crush Zone, the Sanandaj-Sirjan zone (SSZ), and the Urumieh-Dokhtar magmatic arc (UDMA). The Mesopotamian Plain and the Persian Gulf in the southwest are the foreland basin at the front of the orogen. To the northeast lies the SFB [*Falcon*, 1969], consisting of an almost continuous sequence of Paleozoic to the Late Tertiary shelf sediments deposited on the 1–2 km thick infra-Cambrian Hormuz Salt formation overlying a probable Precambrian basement of the northeast margin of the Arabian Platform. Although this basement is not exposed, its age is inferred from 'exotic' metamorphic blocks brought to the surface in salt plugs [*Haynes and McQuillan*, 1974]. The sediments are now deformed into large, range-parallel folds. The folding is oldest and most intense in the northeastern part of the SFB and is more gentle and younger to the southwest [*Alavi*, 1994]. The northeastern limit of SFB is marked by the High Zagros or Crush Zone, a long narrow belt of structural deformation which includes basic intrusive rocks contemporaneous with the late Tertiary folding [*Wells*, 1969]. The high Zagros is separated from the SSZ [*Stocklin*, 1968] to the northeast by the Main Zagros Thrust (MZT) believed to be the suture between the Eurasian and Arabian plates. During much of the Mesozoic, the SSZ represented an active Andean-like margin [*Agard et al.*, 2005]. The SSZ is bounded to the east by the UDMA in which there has been almost continuous volcanic activity from the Eocene to the Pliocene [e.g., *Şengör et al.*, 2008] and is believed to be the Andean-type arc related to the subduction of the Neo-Tethys [*Agard et al.*, 2005]. Other abbreviations: ZFT – Zagros Frontal Thrust; NAF – North Anatolian Fault; EAF – East Anatolian Fault; DSF – Dead Sea Fault; AKBF – Ashgabat Fault.

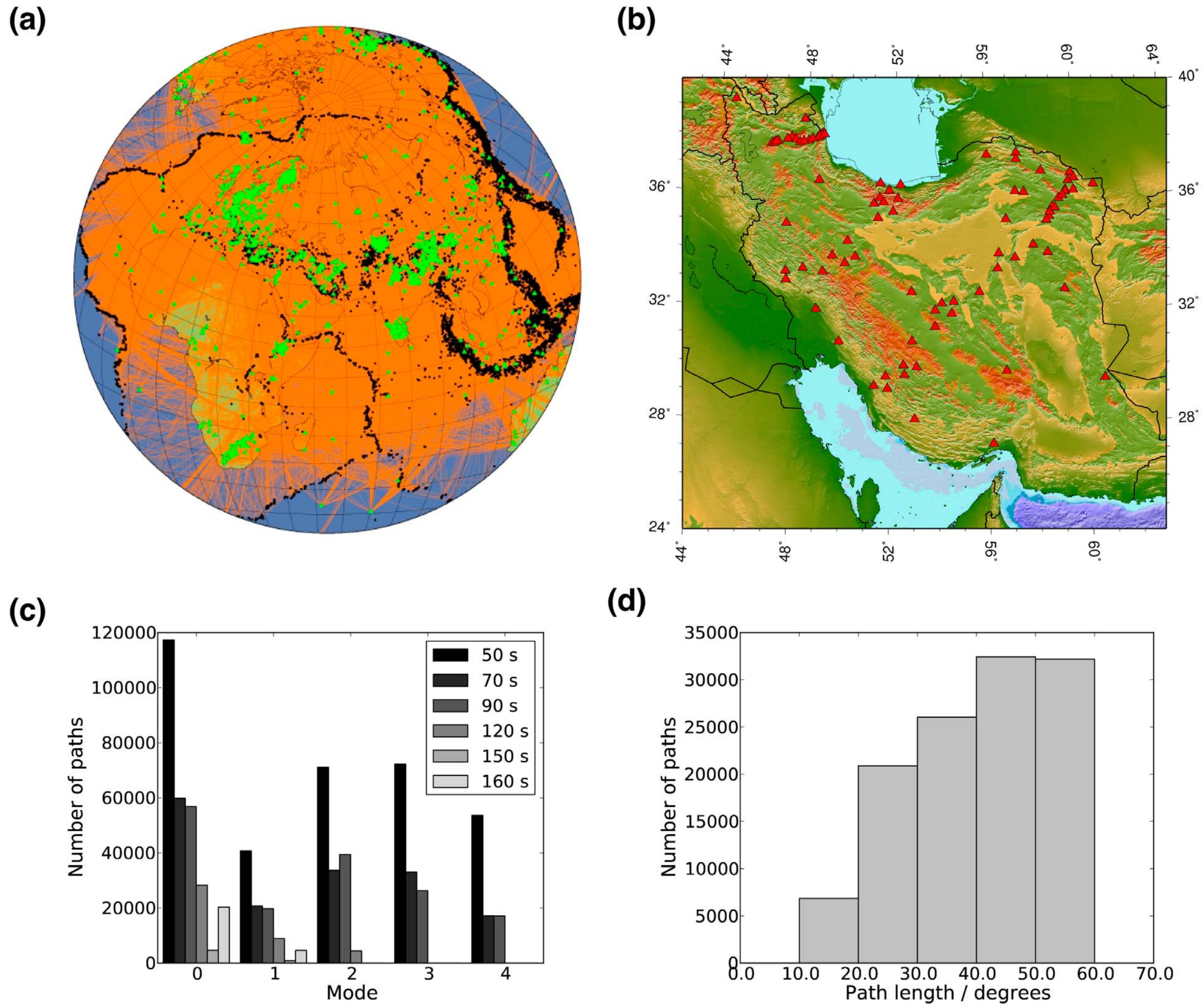

Figure 2. Summary of the surface wave data analyzed. (a) Path coverage is shown in orange with earthquakes shown as black dots and stations as green triangles. (b) Location of the seismographs on the Iranian Plateau providing surface wave data. (c) Frequency and modal content of the surface wave data. The first (black) bar for each mode is the number of measurements at 50 s period. (d) Path length distribution of the data. Path density and azimuthal coverage for the (e) complete data set, (f) fundamental mode, (g) first overtone, (h) second overtone, (i) third overtone and (j) fourth overtone. The path density is denoted by the shading from white (no paths) to black (>1000 paths) per 2° × 2° cell. The red grid overlying the path density maps indicates the Voronoi diagram which is constructed by expanding the cell from an initial 2° × 2° size until an optimized azimuthal spread in each cell is achieved [*Debayle and Sambridge*, 2004]. The 2° cell size over most of the region shows that the azimuthal coverage of the surface wave data is high over the Middle East.

determined for clusters consisting of a large number of paths, and we use these errors in place of $\sigma_M(z)$ determined from a small number of paths.

[10] The average velocity models from the clustered models are then combined in a tomographic inversion to obtain the 3D S_v-wave speed structure and the azimuthal anisotropy as a function of depth using the technique of *Montagner* [1986] as implemented by *Debayle and Sambridge* [2004] for massive data sets. The lateral smoothness of the 3D model is controlled by a Gaussian *a priori* covariance function defined by a scale length L_{corr} which defines the distance to which adjacent points of the model are correlated and acts as a spatial filter; a standard deviation σ controls the amplitude of the perturbation in the Earth structure allowed in the inversion. The tomographic model presented here was determined with L_{corr} = 250 km and σ = 0.05 km s^{-1}.

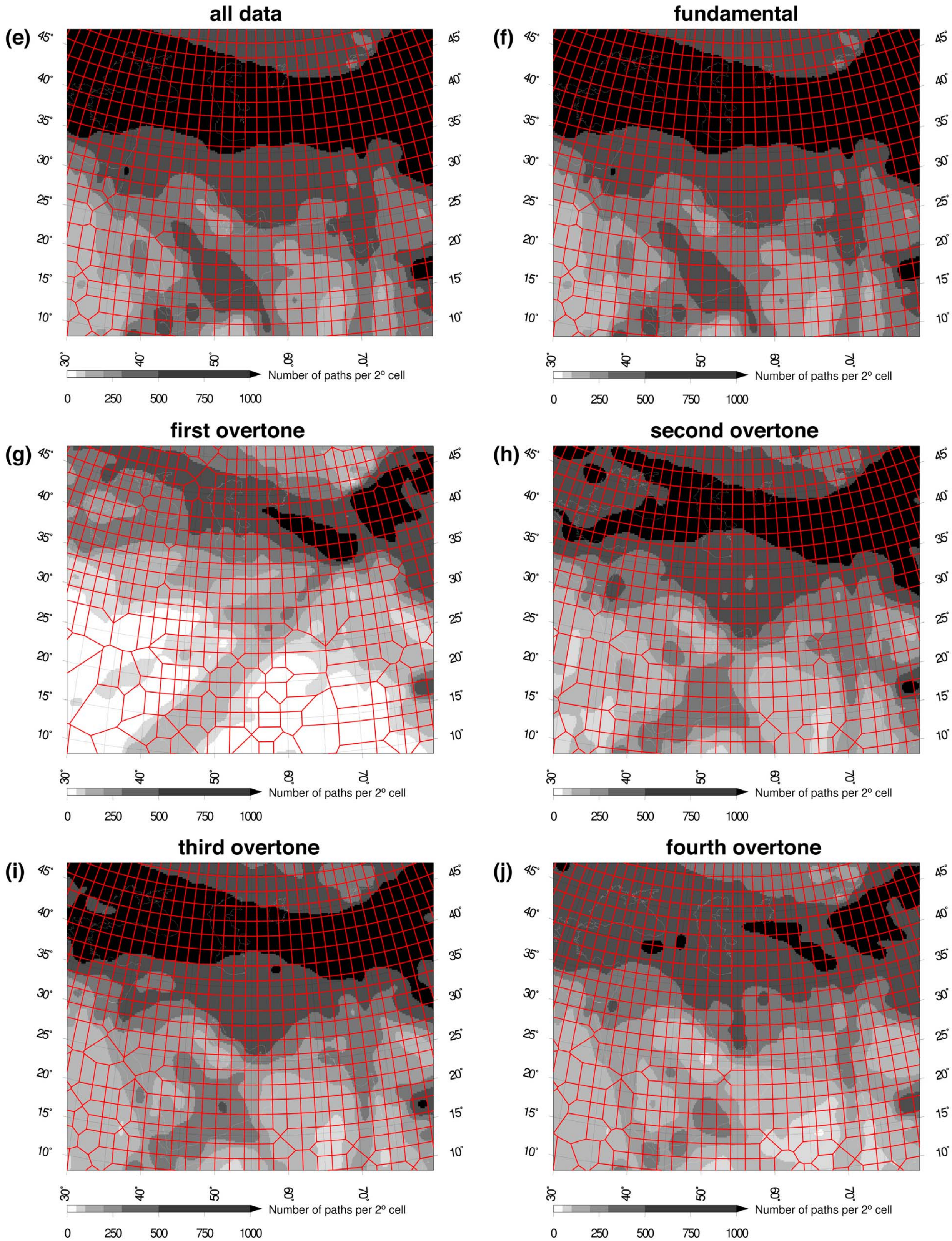

Figure 2. (continued)

2.2. Upper Mantle Velocity Model of the Middle East Region

[11] The upper-mantle V_s model derived from the surface wave analysis is shown in Figure 3 and the resolution tests for the model are discussed in Figure 4. At 75 km depth (Figure 3a) most of the region is slow with respect to the reference velocity at this depth. Very slow wave speeds ($<-7\%$) exist beneath the East Anatolian Plateau and the northwestern part of the Iranian Plateau, below the southern end of the Red Sea and the adjacent parts of Arabia and Africa, and below northern Pakistan and the Hindu Kush. High wave speeds occur beneath the South Caspian Basin and the Turan Shield north of the Iranian Plateau. Wave speeds below the Mesopotamian Foredeep deviate little ($<\pm1\%$) from the reference model. The resolution tests (Figures 4a and 4b) show that both the velocity anomaly amplitudes and geometries are well recovered at 75 km depth.

[12] The velocity structure changes dramatically at 125 km depth (Figure 3b). The slowest wave speed mantle at this depth occurs beneath Afar, west-central Arabia and the East Anatolian Plateau. A restricted area of the eastern Iranian Plateau is moderately slow, but the upper mantle beneath the Mesopotamian Foredeep, the Zagros Mountains and across the Strait of Hormuz into the adjacent part of Arabia is 2–5% fast with respect to the reference velocity. High velocities extend beneath the Caspian Sea. The continuous low-velocity band extending from east Anatolia to the southern end of the Red Sea seen at 75 km depth starts to separate into three low wave speed features at 125 km depth, one beneath east Anatolia, one centered beneath western Arabia, and one at the southern end of the Red Sea and Afar. Another low-velocity feature occurs in the Gulf of Aden between southern Arabia and the Horn of Africa. The resolution tests (Figures 4a and 4b) show that at these depths the geometry of the synthetic anomalies is well recovered and the full amplitude is recovered over most of the anomalies below the Zagros, Central Iran and the Caspian Sea. The amplitude of the anomaly beneath southeastern Arabia is reduced by 30–40%. The cross-sections for the synthetic tests indicate that the vertical resolution at 150 km depth is about $\sim$25 km.

[13] At 175 km depth (Figure 3c) the slow wave speed feature beneath the East Anatolian Plateau is confined to the region south of the East Anatolian Fault. The other three low-velocity features seen at 125 km depth persist at 175 km depth, and the feature below the shield in western Arabia is the lowest velocity anomaly in the region at this depth. The amplitudes of these features are less than those at shallower depths, but the resolution tests (Figures 4e–4h) demonstrate that the amplitude recovery is reduced by $\sim$50% at this depth beneath Arabia. Wave speeds beneath the central Zagros Mountains are as much as 6% higher at 175 km depth, shear wave speeds comparable to those found beneath shields. High velocities extend across the Mesopotamian Foredeep to beneath the Rub-al-Khali Basin in southeastern Arabia. The zone of high velocities below the southern Zagros persists as a weak feature at 250 km depth (Figure 3d), whereas low velocities beneath the Arabian Shield and the Afar persist to at least 250 km depth. Over most of the region the wave speed at this depth differs little ($<\pm1\%$) from the reference model. The resolution tests (Figures 4e and 4f) demonstrate that below 250 km depth the geometry of the synthetic anomalies is reasonably well-resolved but that the amplitudes of the anomalies are severely reduced.

[14] Figures 3e and 3f show cross-sections through the V_s model approximately parallel and perpendicular to the Zagros. At shallow depths the uppermost mantle beneath the Zagros Mountains is slow, but by $\sim$100 km depth the upper mantle wave speeds extending from the northern Zagros ($\sim$36°N,46°E) to the Strait of Hormuz are fast. The fast upper mantle S_v-wave speed persists beneath the Zagros Mountains to about 250 km depth; the S_v-wave speeds beneath the Arabian Platform and the central Iranian Plateau remain slow. The low-wave speed mantle beneath western Arabia has significantly lower V_s-wave speeds than those found beneath the adjacent parts of the Red Sea. Low wave speeds extend to deeper depths at the northwestern end of profile BB′ beneath the East Anatolian Plateau (Figure 3f). This boundary between high shear wave speeds beneath the northern Zagros and low shear wave speeds beneath the East Anatolia Plateau is quite abrupt and extends to at least 200–250 km depth.

2.3. Teleseismic S-Wave Delay Times

[15] Relative teleseismic S-wave delay times measured across the Iranian Plateau reveal a similar strong contrast between the higher upper mantle shear wave velocity beneath the Zagros and the lower shear wave velocity beneath central Iran as does the surface wave tomography (Figure 5). The relative S-wave arrival times are measured using the multichannel cross-correlation method

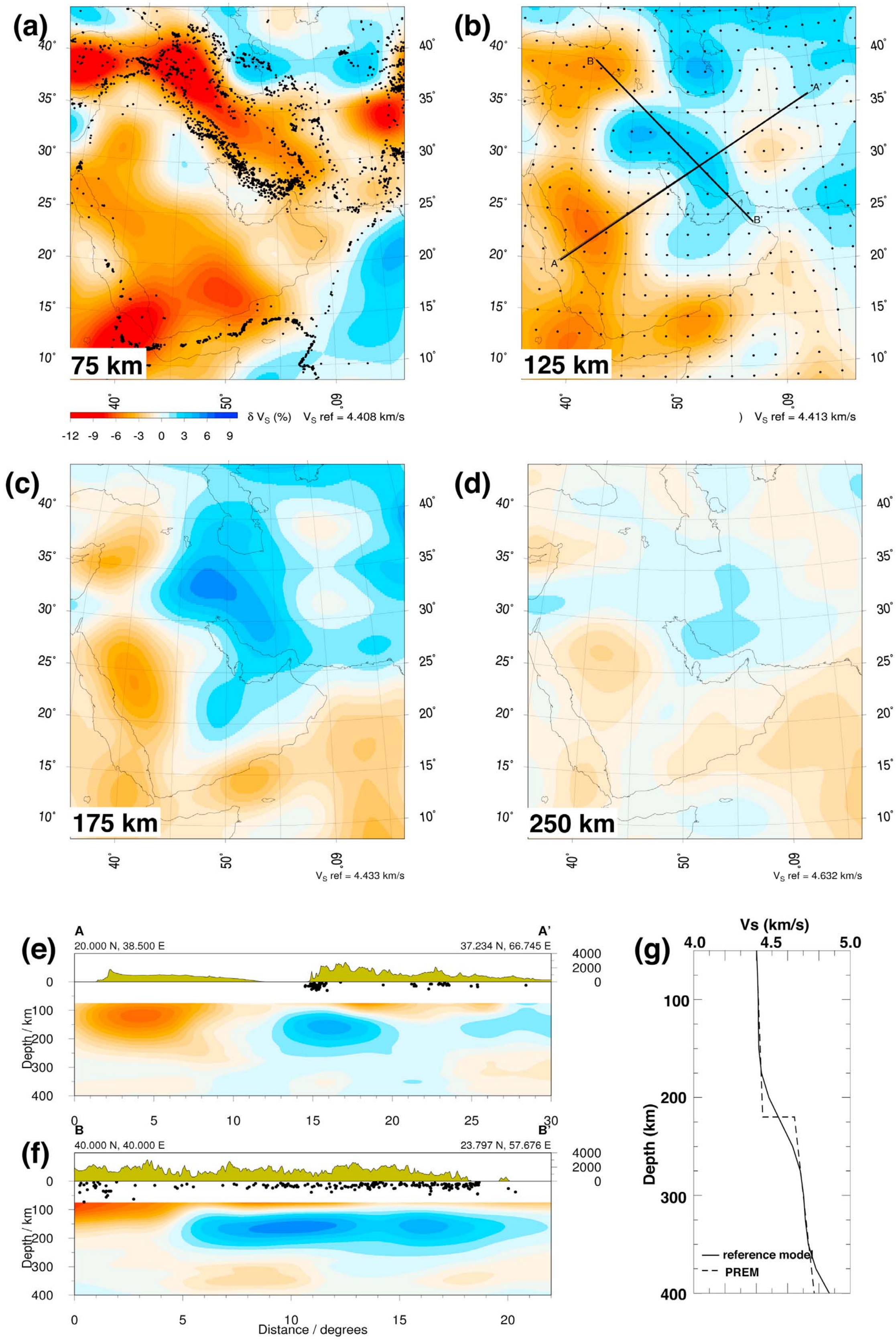
(a)
75 km
δ VS (%) VS ref = 4.408 km/s
-12 -9 -6 -3 0 3 6 9
(b)
125 km
A
A'
B
B'
VS ref = 4.413 km/s
(c)
175 km
VS ref = 4.433 km/s
(d)
250 km
VS ref = 4.632 km/s
(e)
A
20.000 N, 38.500 E
A'
37.234 N, 66.745 E
Depth / km
(f)
B
40.000 N, 40.000 E
B'
23.797 N, 57.676 E
Distance / degrees
(g)
Vs (km/s)
Depth (km)
reference model
PREM

Figure 3

of *VanDecar and Crosson* [1990]. The observed relative residual travel-time for the ith ray is given by

$$\Delta t_i = t_i^{obs} - t_i^{ref} - t_i^{elev} - \langle t_e \rangle,$$

where t_i^{obs} is the observed relative arrival time, t_i^{ref} is the predicted travel-time for the reference model, in this case IASP91 [*Kennett and Enghdal*, 1991], and t_i^{elev} is the elevation correction term for each site. The average event arrival time $\langle t_e \rangle$ is chosen separately for each earthquake so that the mean of the travel-time residuals is zero. Positive residuals indicate a delayed travel time and negative residuals indicate early arrivals with respect to the predicted IASP91 arrival time. Relative residual travel times are compared because absolute arrivals are less accurate in the presence of noise and relative residual travel times minimize any errors due to uncertainties in earthquake origin times.

[16] The teleseismic S-wave residuals for the profile crossing the Iranian Plateau use (Figure 5a) data recorded during the 2000–2001 IIEES-LGIT experiment [*Paul et al.*, 2006] and the 2006–2008 IIEES-UCam experiments [*Nowrouzi et al.*, 2007; *Rham*, 2009; *Motaghi et al.*, 2011, 2012]. Sites occupied in the IIEES-LGIT experiment extend from the edge of the Zagros foreland basin in the southwest, across the Zagros fold-and-thrust belt, the Sanandaj-Sirjan volcanic arc and to the Urumich-Dokhtar magmatic arc to the edge of the central plateau (Figure 1). Sites occupied during the 2006–2008 IIEES-UCam experiments overlap in the central part of the plateau with the easternmost sites of the IIEES-LGIT experiment and extend across the central plateau and Kopet Dagh Mountains to the edge of the Turan Shield (Figure 1).

[17] The S-wave residuals that are uncorrected for lateral variations in crustal structure (Figure 5c) show a long wavelength trend with early arrivals (∼−1 sec) in the southwest and late arrivals (∼+1.5 sec) in the northeast. *Kaviani et al.* [2007] found a similar trend but one of smaller amplitude for relative teleseismic P-delays measured from IIEES-LGIT experiment recordings. Also shown in Figure 5c are S-delays computed for the mantle shear wave model derived from the surface wave tomography. The S-delays computed for the surface wave tomographic model show a similar SW-to-NE trend in delay time with early arrivals in the Zagros as do the observed S-wave residuals uncorrected for crustal structure. After correcting the S-wave residuals for lateral variations in crustal thickness and velocity along the profile (Figure 5d) by using results from crustal receiver function inversions [*Nowrouzi et al.*, 2007; *Rham*, 2009; *Motaghi et al.*, 2011, 2012], we found much earlier arrival times for stations in the Zagros (∼−4 sec), ones that are suppressed in Figure 5c due to the thick (50–55 km) and somewhat slower Zagros crust compared to that in central Iran (35–40 km). The IIEES-LGIT and IIEES-UCam experiments were operated at different times and have no sites in common. However, the results agree where the IIEES-LGIT and IIEES-UCam sites overlap and the large negative relative arrival signal is confined to sites of the IIEES-LGIT experiment.

2.4. Constraints on Upper Mantle Structure of the Middle East From Previous Seismological Studies

[18] The surface wave tomography upper mantle V_s model (Figure 3) for the Middle East shows that a thick, high-velocity upper mantle lid exists beneath the Mesopotamian Foredeep, the Zagros fold-and-thrust belt, the South Caspian and Rub-al-Khali Basins. Teleseismic S-wave delay time differences across the Zagros and the central Iranian Plateau

Figure 3. Horizontal slices through the surface wave tomographic model at (a) 75 km, (b) 125 km, (c) 175 km and (d) 250 km depths. Black dots in Figure 3a show locations of earthquake magnitude 4.5 and greater from *Engdahl et al.* [1998] (updated through 2007). The regular grid of small black dots in Figure 3b denotes the points at which the velocity was determined in the surface wave tomography. The reference velocity at each depth is given at the right beneath the individual maps, the per cent perturbation scale from the reference wave speed is given at left below Figure 3a. Two depth cross-sections (locations shown in Figure 3b) through the surface wave tomographic model approximately (e) perpendicular (A-A′) and (f) parallel (B-B′) to the Zagros Mountains. The velocity perturbation scale below Figure 3a also applies to the depth cross-sections. Each panel of the cross-sections is split into three sections: an upper section showing the topography along the profile, a central section from sea level to 75 km depth where earthquakes within ±100 km of the profile are plotted, and a lower section showing the shear wave velocity perturbation of the surface wave tomographic model. Note the different vertical scales for elevation above sea level and depth below sea level. (g) The reference shear-velocity model (solid line) is based on PREM [*Dziewonski and Anderson*, 1981] (dashed line) but with the PREM discontinuities at 220 and 410 km depth smoothed. The velocity perturbation at each depth shown in the cross-sections is plotted with respect to the reference model velocity at that depth.

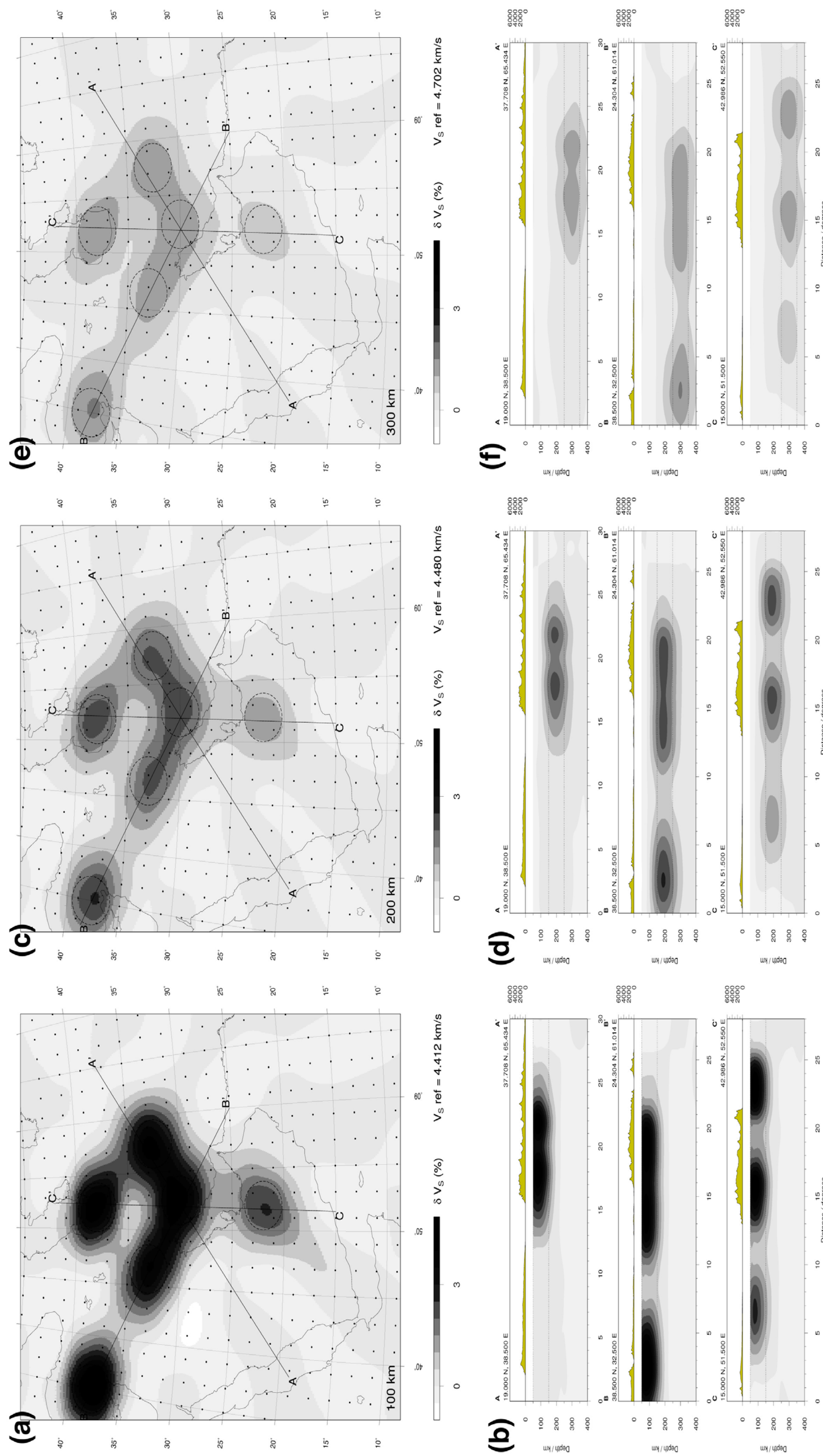
(a)
100 km
δ V_S (%)
V_S ref = 4.412 km/s
(b)
(c)
200 km
V_S ref = 4.480 km/s
(d)
(e)
300 km
V_S ref = 4.702 km/s
(f)
Depth / km
Distance / degrees

Figure 4

confirm the existence of the high velocities beneath the Zagros orogen. The shear wave speeds observed in the high velocity lid are comparable to those seen in the upper mantle beneath most of the Archean shields. Beneath the rest of the region, a high-velocity lid is either quite thin or absent altogether. In the model, very low shear wave speeds extend to depths of several hundred kilometers beneath the East Anatolian Plateau, the west-central part of the Arabian Shield and the Afar region.

[19] A number of the large-scale features seen in Figure 3 have been previously noted, but they are not at the same resolution or scale. Early fundamental mode Rayleigh wave phase velocity measurements [*Asudeh*, 1982] demonstrated that at 100 km depth, V_s varied from 4.24 km s^{-1} beneath northern Iran, 4.65 km s^{-1} below central Iran and 4.98 km s^{-1} beneath the Zagros. The surface-wave tomographic study of *Maggi and Priestley* [2005] found a low shear wave velocity (<4.5 km s^{-1}) in the uppermost mantle (100 km depth) beneath the East Anatolian and central Iranian Plateaus and a high shear wave velocity beneath the bounding region of the Arabian plate. Fundamental mode Rayleigh wave phase velocity measurements by *Kaviani et al.* [2007] found that, beneath the Zagros, V_s varied from 4.5 ± 0.2 km s^{-1} below the Moho to 4.9 ± 0.25 km s^{-1} at 200 km depth. They observed that beneath the suture region from the Main Zagros Thrust (MZT) to the UDMA, shear wave velocities at shallow depths are somewhat lower than those beneath the Zagros with a minimum of 4.4 ± 0.2 km s^{-1} at $\sim$80 km depth, but at depths of 150 km and deeper, the shear wave velocities are as high as those beneath the Zagros. All these features are seen at a broader scale in our upper mantle V_s model.

[20] The Arabian Peninsula has been the focus of several surface wave studies. *Rodgers et al.* [1999] examined surface wave propagation across the Arabian Shield and Platform and concluded that P- and S-wave speeds immediately below the Moho are slower in the Arabian Shield than in the Arabian Platform (7.9 and 4.30 km s^{-1} and 8.1 and 4.55 km s^{-1}, respectively). *Tkalčić et al.* [2006] found significant variations in high velocity lid thickness and anomalously low shear wave velocities beneath the Arabian Shield and *Park et al.* [2008] observed shear wave velocities as low as 4.2 km s^{-1} at $\sim$150 km depth beneath the Shield. *Debayle et al.* [2001] demonstrated that low shear wave velocities exist in the upper mantle beneath the Afar and the surrounding region similar to those seen in Figure 3. These observations compare favorably to the difference in upper mantle V_s we find between the Arabian Shield and Platform (Figure 3).

[21] *Hansen et al.* [2007] and *Angus et al.* [2006] used S-receiver functions to measure upper mantle lid thickness in the Arabian Peninsula and Eastern Turkey, respectively. To model the arrivals assumed to be from the base of the lid, *Hansen et al.* [2007] required sub-lid shear wave velocities of about 4.2 km s^{-1}. Near the Red Sea coast, the base of the lid is at a depth of about 50 km; however, it rapidly deepens to attain a maximum depth of about 120 km beneath the Arabian Shield within 300 km of the Red Sea. At the Shield-Platform boundary, they observed a step in the lid thickness where the depth increases rapidly to about 160 km in the region where we see higher shear wave velocities beneath parts of the Rub-al-Khali Basin. *Angus et al.* [2006] observed phases in the S-receiver functions from the northern Arabian Shield and

Figure 4. We conduct synthetic tests to determine how well the tomography recovers the shapes and amplitudes of given distributions of shear velocity heterogeneity. These tests provide an estimate of how well features in the observed tomography model are resolved. The input model consists of 500-km diameter by 100-km thick circular plates having a +10% wave speed variation superimposed on a smooth background model (Figure 3g). Six plates were located in each depth range: (a and b) 50–150 km, (c and d) 150–250 km and (e and f) 250–350 km depths. The geographic location of the plates is best seen in Figure 4e. The depth extent of the plates is denoted by the dashed lines in Figures 4b, 4d, and 4f. We calculate synthetic multimode seismograms for these velocity models for the same source parameters (location, mechanism and moment) and event–receiver combinations as for the observed seismograms. The synthetic seismograms are then inverted in the same way as the real data. By starting with the initial step of the 1D waveform inversions, our tests not only provide insights on the spatial resolution of the model attained from the path coverage, but they also yield information on the depth resolution attained from the frequency and modal content of the seismograms analyzed. The geometry of all plates is recovered although there is some smearing between some of the plates. At 50–150 km depth (Figures 4a and 4b) nearly the full amplitude is recovered for the anomalies located beneath the Zagros, central Iran and the Kopet Dagh and the South Caspian Basin, but the amplitude of the plate below southeastern Arabia is reduced by $\sim$30–40%. With the plates at 150–250 km depth (Figures 4c and 4d) the amplitude of the anomalies beneath the Zagros, central Iran and the Kopet Dagh and the South Caspian Basin is reduced by $\sim$50%, and the amplitude of the anomaly below southeastern Arabia is reduced by $\sim$70%. With the plates at 250–350 km depth (Figures 4e and 4f) the synthetic anomalies are spatially resolved, but the amplitudes of the anomalies are severely reduced. Depth resolution varies from about $\sim$25 km at 150 km depth to better than $\sim$50 km at 350 km depth.

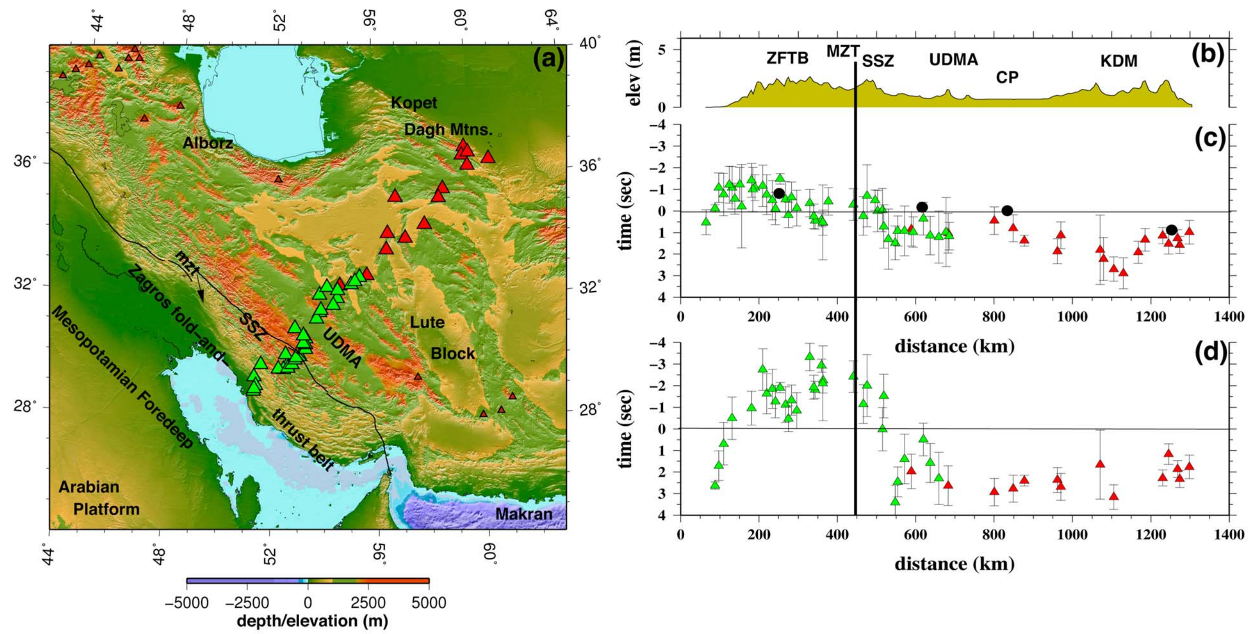

Figure 5. Teleseismic S-wave residual profile across the Iranian Plateau. (a) Map showing locations of the sites whose data are used in measuring the relative S-wave residuals. Sites marked as green triangles are from the 2000–2001 IIEES-LGIT seismic experiment; sites marked by red triangles are from the 2006–2008 IIEES-UCam seismic experiment. Orange triangles are sites of Quaternary volcanoes. (b) Variation in topography along the profile. Abbreviations: ZFTB – Zagros fold-and-thrust belt, MZT – Main Zagros Thrust, SSZ – Sanandaj-Sirjan Zone, UDMA – Urumieh-Dokhtar magmatic arc, CP – central plateau, and KDM – Kopet Dagh Mountains. (c) Relative S-wave residuals uncorrected for crustal thickness and velocity variations. Green and red triangles denote the same IIEES-LGIT and IIEES-UCam sites on the map. Black dots denote the relative S-wave residuals computed through the surface wave tomography model (Figure 3). (d) Relative S-wave residuals corrected for crustal thickness and velocity variations. The heavy black vertical line extending across Figures 5b–5d denotes the location of the MZT. Positive residuals indicate a delayed travel time while negative residuals indicate an advanced travel time.

Iranian Plateau, indicating that the base of the lid for these regions is at 100–125 km depth and that eastern Turkey has an anomalously thin (between 60 and 80 km) upper mantle shear wave speed lid.

[22] Propagation characteristics of the regional seismic phases P_n and S_n, which bottom in the uppermost mantle, provide important information on upper mantle lid structure in a shallow depth range where the vertical resolution of the long-period surface waves is poor. High P_n wave speeds (8.1–8.4 km s^{-1}), similar to the high P_n wave speeds observed for shields [*Christensen and Mooney*, 1995], occur beneath the central and eastern Arabian plate, the South Caspian Basin and the Zagros to the southwest of the suture [*Hearn and Ni*, 1994; *Al-Lazki et al.*, 2004]. Low (<8.0 km s^{-1}) to very low (<7.8 km s^{-1}) P_n wave speeds occur beneath central Iran, the East Anatolian Plateau and a zone running from east Anatolia to the northern part of the Red Sea and then southward through western Arabia [*Hearn and Ni*, 1994; *Al-Lazki et al.*, 2004]. The sharp P_n velocity contrast across the Bitlis-Zagros suture indicates the presence of a stable Arabian mantle lid south of the suture and suggests that the Arabian plate is not underthrusting the East Anatolian Plateau and that the suture extends down to the uppermost mantle [*Al-Lazki et al.*, 2003].

[23] Efficient S_n propagation implies the presence of a high-velocity mantle lid with a positive velocity gradient with depth such as that found beneath shields, while inefficient S_n propagation implies high temperatures in the uppermost mantle and the possible presence of some melt [*Molnar and Oliver*, 1969]. S_n studies for the Middle East [*Kadinsky-Cade et al.*, 1981; *Rodgers et al.*, 1997; *Sandvol et al.*, 2001; *Gök et al.*, 2003; *Al-Damegh et al.*, 2004] find that propagation is efficient for paths confined to the eastern parts of the Arabian Plate, including the Zagros, but S_n is blocked for paths crossing northern and central Iran east of the MZT and for paths crossing western Arabia beneath the shield where the surface wave tomography model shows very slow upper mantle S_v-wave speeds. S_n is not observed in eastern Turkey and

is attenuated immediately beneath and to the east of the Dead Sea Fault zone [*Al-Lazki et al.*, 2003; *Al-Damegh et al.*, 2004]. South of the East Anatolian Fault Zone, S_n attenuation is high even though P_n velocities are normal. Across the Bitlis suture zone there is a sharp transition from efficient S_n propagation to the south to blocked S_n to the north. These S_n propagation characteristics are consistent with our S_v model at deeper depths that show a thick upper mantle, high-velocity lid with a positive gradient with increasing depth beneath the Zagros orogen. The S_n observations indicate that a high-velocity lid with a positive velocity gradient with depth must exist beneath the Arabian Platform, but this places no constraint on its thickness. If a high-velocity lid exists beneath the Arabian Shield, the East Anatolian Plateau or the central Iranian Plateau, it must be very thin or have a negative velocity gradient with depth.

3. The Zagros Core

[24] To map the lithospheric thickness beneath the Middle East we convert the shear wave speed *vs.* depth profiles of our seismic model to temperature *vs.* depth profiles. Various ways of relating seismic wave speed and temperature have been proposed [e.g., *Goes et al.*, 2000; *Shapiro et al.*, 2004; *An and Shi*, 2006], most of which are based on assumptions of the rheological properties and grain size and their relationship to seismic velocity. Here we use a parametrization $T(V_s, z)$ similar to that of *Priestley and McKenzie* [2006] which makes no such assumptions. Figure 6 shows the temperature estimate determined from the tomographic model at a depth of 125 km beneath the Middle East. The upper mantle potential temperature beneath mid-ocean ridges is 1330 ± 20°C [*White et al.*, 1992]. Adding 75°C which corresponds to an isentropic gradient of 0.6°C/km, the real temperature estimate at 125 km depth is 1405 ± 20°C. The solidus at this depth is 1595°C. The temperature at 125 km depth is significantly less than 1405°C beneath the Zagros, the Mesopotamian Foredeep, the Rub-al-Khali Basin and the South Caspian Basin. The temperature is significantly greater than 1405°C beneath the Afar region and the belt extending from Yemen, through the Arabian Shield, parts of Jordan and Syria to eastern Anatolia and below the central part of the Iranian Plateau.

[25] Temperature profiles as a function of depth derived from the surface wave tomography model were fit with a geotherm in the manner described by *McKenzie et al.* [2005], revealing the depth at which the change in temperature gradient occurs at the base of the lithosphere. Comparisons between surface-wave-derived estimates of lithospheric thickness and those estimated from upper mantle nodule mineralogy for southern Africa demonstrate that they agree to within ∼25 km [*Priestley and McKenzie*, 2006; *McKenzie and Priestley*, 2008]. However, because the crust and very shallow upper mantle structure are not well resolved by the long-period surface waves analyzed in Section 2, the geotherms determined from the seismic wave speeds are accurate only for lithospheric thicknesses greater than about 120 km.

[26] For most of the Middle East the lithosphere is thin (<120 km). However, there is a region below the Zagros Mountains and Mesopotamian Foredeep where the lithosphere reaches a thickness of more than 225 km (Figure 7). Lithosphere that is 180–200 km thick extends beneath the South Caspian Basin and a tongue of thickened lithosphere protrudes across the Persian Gulf from the southern Zagros to below the Rub-al-Khali Basin in the southeastern part of the Arabian Peninsula. With the exception of the Rub-al-Khali Basin, only an upper bound of ∼120 km can be given for the depth to the base of the lithosphere below the Proterozoic Arabian Platform and Shield. Thick lithosphere has normally been associated with continental cratons, but it is also found beneath the Himalaya and Tibet orogen [*Priestley et al.*, 2006]. Because thick lithosphere is not confined to merely the upper mantle below the ancient parts of the continents, *Priestley and McKenzie* [2006] suggested using the term 'cores' rather than 'cratonic roots.' We will refer to the thick lithosphere beneath the Zagros as the 'Zagros core.'

[27] The Zagros Mountains are the active fold-and-thrust belt on the leading edge of the Arabian plate. Shortening in the Zagros crust is accomplished by a combination of folding in the sediments [*Sattarzadeh et al.*, 1999], high-angle thrust faulting in the basement [*Jackson*, 1980; *McQuarrie*, 2004], and thickening of the lower crust [*Hatzfeld et al.*, 2003; *Paul et al.*, 2006]. Models proposed for the Zagros mantle include a rigid aseismic Arabian lithosphere sliding beneath the Zagros orogen [e.g., *Snyder and Barazangi*, 1986] or lithospheric slab break-off and foundering [e.g., *Molinaro et al.*, 2005]. Figure 7 suggests that the lithosphere of the Arabian plate has thrust beneath the Zagros, but rather than being rigid, it has deformed and thickened significantly and now forms a thick lithospheric root beneath the orogen. This cool, thickened lithosphere has not delaminated.

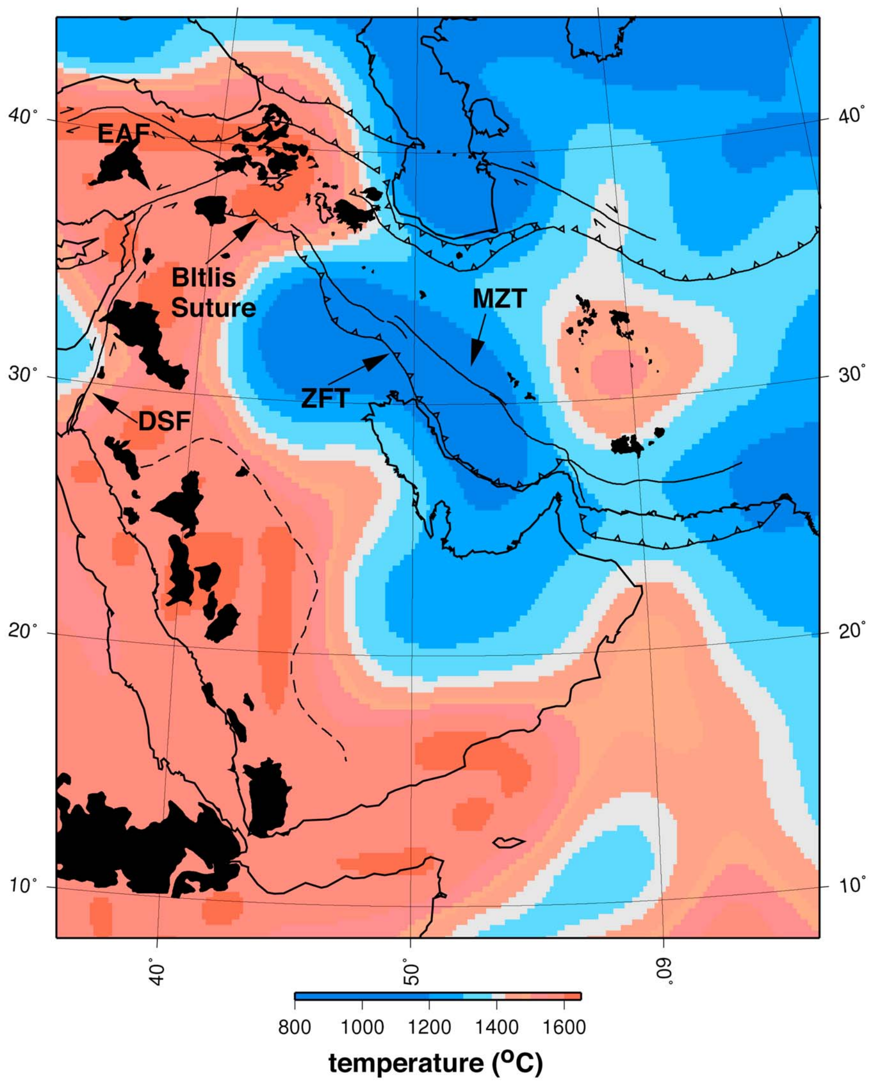

Figure 6. Contours of temperature at 125 km depth beneath the Middle East from the surface wave tomography model using a parametrization $T(V_s, z)$ similar to that of *Priestley and McKenzie* [2006]. The upper mantle potential temperature beneath mid-ocean ridges is 1330 ± 20°C [*White et al.*, 1992]. Adding 75°C which corresponds to an isentropic gradient of 0.6°C/km, the real temperature at 125 km depth is 1405 ± 20°C. The solidus at 125 km depth is 1595°C. In comparison to 1405°C, the mantle at this depth is cool beneath the Zagros orogen, the South Caspian Basin, the Rub-al-Khali Basin and the Turan Shield. Black areas denote locations of recent volcanic fields, mostly younger than 12 Ma [*Camp and Roobol*, 1989; *Sen et al.*, 2004; *Stocklin and Naloavi*, 1971].

[28] The widespread volcanism over the Middle East (Figure 6) also suggests a warm upper mantle as the cause for the low shear wave velocities. The composition of the magmas for these volcanics is controlled by the composition of their mantle source region. D. McKenzie and K. Priestley (The planform of convection beneath the Middle East, equatorial and northern Africa, submitted to *Earth and Planetary Science Letters*, 2012) obtained models of melt generation by inverting rare earth element (REE) concentrations in samples from a number of these volcanic fields. Their inversions show that the very recent volcanics erupted along a belt stretching from Yemen at the southern end of the Red Sea northward to eastern Anatolia can be produced by decompression melting of an asthenospheric source, principally in the transition zone from garnet to spinel peridotite, (~70–90 km depth range). This is consistent with the lithosphere being less than 120 km thick beneath this region. The close resemblance of these magmas to ocean island basalts (OIB) has been pointed out in a number of

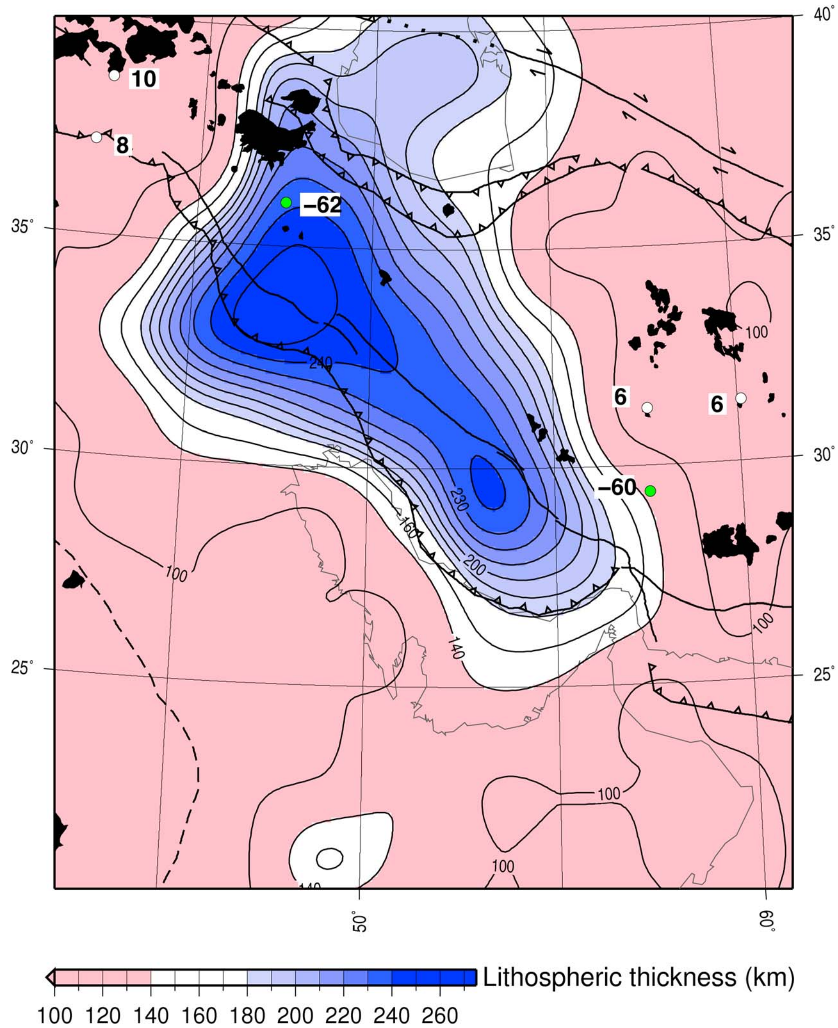

Figure 7. Contours of lithospheric thickness obtained from the shear wave model (Figure 3) by converting the $V_s(z)$ profiles to $T(z)$ and then fitting a geotherm in the manner described by *McKenzie et al.* [2005]. Black areas denote locations of recent volcanics as in Figure 6. Dots denote sites of volcanic samples (white – fertile, green – depleted) used to estimate the source densities of the magmas by analysis of their modal compositions. The numbers in white boxes are the source density differences from MORB ($\Delta\rho = \rho_s - \rho$(MORB) in kg m^{-3} where ρ_s is the source density and ρ(MORB) = 3.323 kg m^{-3} is the density of the MORB source) from McKenzie and Priestley (submitted manuscript, 2012). All densities are calculated at 70 km depth and a temperature of 1000°C and thus $\Delta\rho$ depends only on the source composition and not the temperature.

studies [e.g., *Shaw et al.*, 2003] and, like OIBs, no depletion of the source regions of these basalts is required. Temperatures of the magma source regions are consistent with the upper mantle temperatures shown in Figure 6.

[29] *Walker et al.* [2009] inverted REE concentrations from young (2–5 Ma) volcanic rocks from the central part of the Iranian Plateau (Figure 6). They found that the composition of these volcanic rocks was typical of OIBs and, therefore, they were not from melting of the continental lithosphere. The observed REE concentrations require a small enrichment of a peridotite source within the garnet stability field followed by melting within the spinel stability field (<80 km depth). Again, this is consistent with thin lithosphere beneath central Iran. *Walker et al.* [2009] point out that such volcanic rocks are widespread within eastern and central Iran, but do not occur southwest of a NW-SE trending line to the north of the Zagros, the area where the surface wave tomography shows the lithosphere to be greater than ~120 km. However, there are several small, young volcanic fields on the Iranian Plateau above the region of thick

lithosphere (Figure 7). Because of the extreme enrichment of the light REE in these volcanic rocks, McKenzie and Priestley (submitted manuscript, 2012) believed them to be produced by melting depleted continental lithosphere and not from the convecting upper mantle.

[30] Because their scheme models the behavior of major, minor and trace elements, as well as that of the modal mineralogy, McKenzie and Priestley (submitted manuscript, 2012) were able to calculate the density of the magma source regions. They found that the densities of all the magma source region they analyzed were close to that of MORB with the exception of the Iranian volcanics from above the region of thick lithosphere. Not only did these volcanic rocks show a depleted source region, their densities were much less than MORB (Figure 7). Rocks with such densities will sink into the mantle (delaminate) only if their potential temperature is less than ~900°C. As the densities for these show, this cool lithospheric root beneath the Zagros is stabilized against convective removal because it is depleted. If the temperature of the thickened mantle root was sufficiently cool for it to be convectively unstable, ~900°C, its viscosity would increase by ~10^4 times that of the background upper mantle. This difference will also make convective removal more difficult and therefore will also stabilize the lithosphere. Although recent volcanics are widespread over the Middle East, it is only these volcanics from above the Zagros core which show a low density, depleted source.

4. Summary and Discussion

[31] We use a large, multimode surface wave data set to determine lateral variations in upper mantle shear wave velocity beneath the Middle East. Below most of the region the upper mantle shear wave speed is lower than that of the global average, but at 100–225 km depths beneath the Mesopotamian Foredeep and the Zagros Mountains, the shear wave velocities are comparable to those found beneath the Archean cratons. The lateral variations in wave speed structure observed in the surface wave tomography model are consistent with other seismological observations. For example, the variations in relative teleseismic S-wave arrival times across Iran show advances of as much as 4 sec for the Zagros with respect to the Iranian Plateau. The propagation of the regional seismic phase S_n is inefficient or blocked over much of the Middle East but propagates efficiently within the eastern parts of the Arabian plate and the Zagros.

[32] Using a $T(V_s,z)$ relation similar to that of *Priestley and McKenzie* [2006], we find the upper mantle temperatures at 125 km depth beneath the Afar, the Arabian Shield, parts of Syria and Jordan, eastern Anatolia and central Iran are greater than 1405 ± 20°C, but are very low at this depth beneath the Mesopotamian Foredeep, the Zagros and the South Caspian Basin. The upper mantle temperatures derived from the seismic model are consistent with upper mantle temperatures derived from modeling the geochemistry of the volcanics in the region. Fitting temperature *vs* depth profiles with a geotherm allows us to determine the depth where heat transport changed from advection in the deeper mantle to conduction in the shallower mantle. This depth corresponds to the base of the lithosphere. The lithosphere is thin (<120 km) beneath most of the Middle East but a thick lithospheric keel extending to as much as 225 km depth exists beneath the Mesopotamian Foredeep and the Zagros Mountains. Geochemical modeling of young volcanics from above the Zagros core shows they are small lithospheric melts and the density of their source region is ~60 kg m^{-3} less than fertile mantle, whereas the source region densities for magmas above regions of thin lithosphere are close to that of fertile mantle. Thus, the cool, thickened lithosphere beneath the Zagros Mountains and Mesopotamian Foredeep is stabilized from delamination by depletion.

[33] The spatial pattern of SKS-splitting in the Middle East is complex (Figure 8) and this complexity seems related to the Zagros Core. The observation that in many continental regions SKS-splitting patterns appear to be spatially related to geologic and tectonic features has led some [e.g., *Silver*, 1996] to suggest that the anisotropy responsible for the splitting exists largely in the continental lithosphere and is a result of recent, significant tectonic events. Others contend that this correlation results from complex patterns of mantle flow that are related to 3-D morphology of the lithospheric mantle [e.g., *Bormann et al.*, 1996]. In the Middle East the strongest SKS-splitting is observed in regions of thin lithosphere and little or no splitting occurs in the region of the thick lithosphere below the Zagros orogen (Figure 8). We have only an upper bound of ~120 km on the lithospheric thickness in the central Iranian Plateau where receiver function measurements show the crust is 40–45 km thick [*Nowrouzi et al.*, 2007; *Rham*, 2009; *Motaghi et al.*, 2011, 2012]. Therefore, the thickness of the mantle layer of the lithosphere is probably <70 km. If the 1–2 s splitting observed in the central Iranian Plateau is

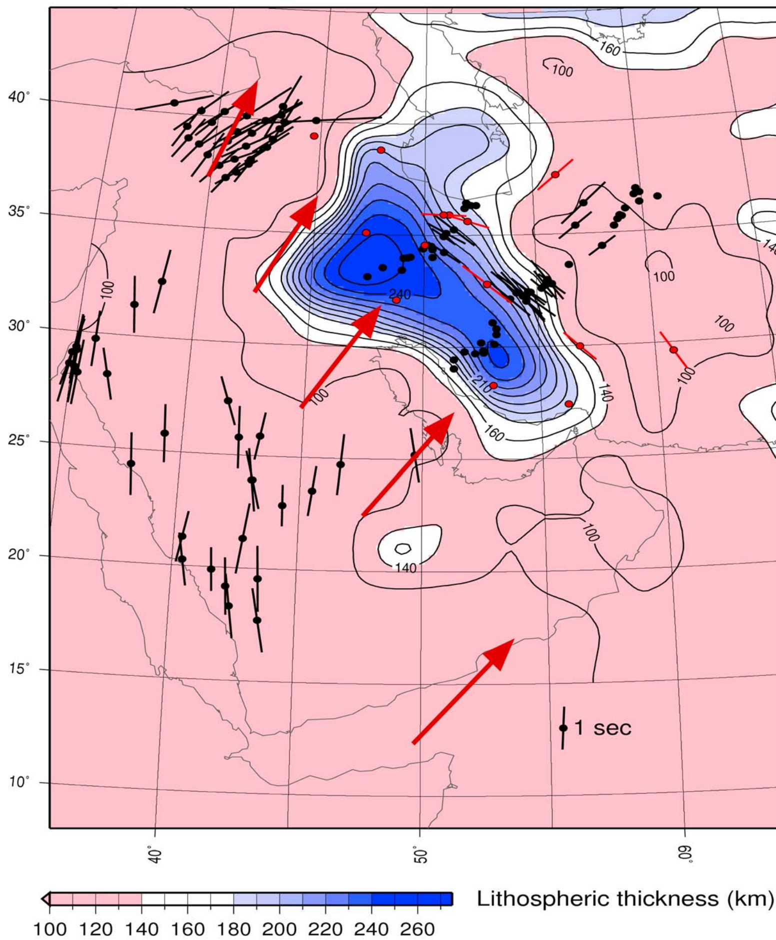

Figure 8. SKS-splitting measurements for the Middle East plotted on a contour map of lithospheric thickness. Solid red circles indicate locations of permanent seismograph sites and black circles indicate locations of temporary seismograph sites. Lines extending from the circles denote the fast SKS-polarization directions measured at the site. The large red arrows indicate the motion of Arabia relative to Eurasia (model NNR-NUVEL-1A). The SKS-splitting scale is in the lower right part of the map. Beneath Arabia [*Hansen et al.*, 2006] the fast SKS-polarization directions are uniform and approximately N-S. The fast SKS-polarization directions in eastern Anatolia [*Sandvol et al.*, 2003] are relatively uniform and exhibit primarily NE-SW orientations. The fast SKS-polarization direction pattern for the Iranian Plateau [*Kaviani et al.*, 2009] is complex but coherent at the scale of a single province. No significant splitting is observed for sites in the Zagros, the SSZ and UDMA. A very short distance to the east of the UDMA the SKS-splitting changes dramatically with the fast arrival oriented $\sim$120° with a 1–2 s lag between the fast and slow arrivals. The transition between the two regimes is sharp and coincides with the northeastern edge of the Zagros core. The SKS-splitting observations of *Kaviani et al.* [2009] consist of measurements from both long-duration permanent stations and short-duration temporary stations. The few measurements per site from the temporary stations are consistent with the larger number of measurements per site made at the permanent stations. The fast polarization directions do not coincide with the absolute plate motion which *Kaviani et al.* [2009] suggest is evidence that the anisotropy responsible for the splitting is in the lithosphere. In relation to the Zagros core, the fast direction of SKS-splitting wraps around the core but indicates that within the core, the anisotropy is either vertical or heterogeneous.

the result of anisotropy in the mantle layer of the lithosphere, 13% or higher anisotropy is required. While such large anisotropy is possible, the variation in SKS-splitting in the central Iranian Plateau suggests to us that, as for Europe [*Bormann et al.*, 1996] and North America [*Fouch et al.*, 2000], the anisotropic source of the observed SKS-splitting below the central Iranian Plateau is likely to be located in the asthenosphere, and the topography of the Zagros core may distort the large-scale asthenospheric flow pattern.

[34] Much of the geological and geophysical observations for the Iranian and East Anatolian Plateaus have been attributed to break-off of the

Neo-Tethys Oceanic slab [e.g., *Şengör et al.*, 2003; *Keskin*, 2003; *Molinaro et al.*, 2005; *Omrania et al.*, 2008; *Hatzfeld and Molnar*, 2010; *Agard et al.*, 2011]. There is evidence in P-wave tomography images [*Lei and Zhao*, 2007; *Zor*, 2008] for high velocity features in the upper mantle below parts of the Iranian and East Anatolian Plateaus and these features have been interpreted as foundered remnants of detached oceanic slabs. However, the proposed recent slab break-off of continent-ocean transitional lithosphere beneath the Zagros Mountains [e.g., *Molinaro et al.*, 2005] or lithospheric thickening with partial delamination to the northeast of the Zagros [e.g., *Hatzfeld and Molnar*, 2010] is at odds with the seismological observations presented here which show a thick lithospheric root now underlying the Zagros, and geochemical modeling of young volcanics in the Zagros which shows that these are lithospheric melts and that the root is composed of depleted material (McKenzie and Priestley, submitted manuscript, 2012).

[35] *Şengör and Kidd* [1979] point out the similarities between the East Anatolian and the Iranian Plateaus. Both regions are seismically active [e.g., *Turkelli et al.*, 2003; *Talebian and Jackson*, 2004] but, unlike the Iranian Plateau, the East Anatolian Plateau does not have a well-developed fold-and-thrust belt as exists in the Zagros. This could be a reflection of the difference in upper mantle structure beneath the two regions resulting in different basal boundary conditions – a thick lithospheric core beneath the Zagros fold-and-thrust belt and a thin or possibly missing lithospheric mantle beneath the East Anatolian Plateau.

[36] There are features of the Arabian-Eurasian collision that are similar to those of the Indo-Eurasian collision, but there is a striking difference in the heights of the Zagros (~2–3 km elevation) and the Himalaya (~5 km elevation) Mountains. This difference probably results from the more advanced stage of the Indo-Eurasian collision compared to the Arabian-Eurasian collision. On the other hand, the elevation difference could result from differences in the strength of the bounding lithosphere as proposed by *Maggi et al.* [2000a]. Lithospheric thickening is occurring beneath the Zagros Mountains (Figure 7) and beneath the Himalaya Mountains and southern Tibet [*Priestley et al.*, 2006]. The lithosphere beneath Arabia to the west of the Zagros is less than ~120 km thick whereas that beneath northern India to the south of the Himalayas is ~200 km or more thick. *Maggi et al.* [2000a] estimated that the elastic thickness (T_e) for northern India supporting the 4–5 km elevation of the Himalaya was 37 km. The T_e of eastern Arabia supporting the ~2–3 km elevation of the Zagros is not well constrained [*Maggi et al.*, 2000a] but is ~30 km. The buoyancy force needed to support the Himalaya is on the order of 5×10^{12} N m^{-1} [e.g., *Molnar and Lyon-Caen*, 1988] whereas the buoyancy force required to support the Zagros is of the order 2.5×10^{12} N m^{-1}. While T_e for the Himalayan and Mesopotamian foredeep is not significantly different, the hinterland of the Himalayan foredeep, southern India, has thick lithosphere extending for a great distance south of the collision zone. In comparison, the hinterland of the Mesopotamian foredeep, the Arabian plate, has a smaller extent of thin lithosphere. In addition, the eastern margin of the Arabian Platform was stretched in the Mesozoic [*Koop and Stoneley*, 1982]. For these reasons, the Arabian plate may be too weak to support elevations higher than that of the present Zagros Mountains.

Acknowledgments

[37] A number of the figures were prepared using the Generic Mapping Tool [*Wessel and Smith*, 1995]. Some of the data obtained from within Iran were recorded on seismographs from SEISUK. We thank Denis Hatzfeld and Anne Paul for sharing data from the LGIT seismic experiments in the Zagros Mountains. We thank Celal Şengör, Andreas Fichtner, Thorsten Becker and James Jackson for constructive, thoughtful reviews. This is Cambridge University Department of Earth Sciences contribution 2603.

References

Agard, P., J. Omrani, L. Jolivet, and F. Mouthereau (2005), Convergence history across Zagros (Iran): Constraints from collisional and earlier deformation, *Int. J. Earth Sci.*, *94*, 401–419, doi:10.1007/s00531-005-0481-4.

Agard, P., J. Omrani, L. Jolivet, H. Whitechurch, B. Vrielynck, W. Spakman, P. Monie, B. Meyer, and R. Wortel (2011), Zagros orogeny: A subduction-dominated process, *Geol. Mag.*, *148*, 692–725, doi:10.1017/S001675681100046X.

Alavi, M. (1994), Tectonics of the Zagros orogenic belt of Iran: New data and interpretations, *Tectonophysics*, *229*, 211–238, doi:10.1016/0040-1951(94)90030-2.

Al-Damegh, K., E. Sandvol, A. Al-Lazki, and M. Barazangi (2004), Regional seismic wave propagation (Lg and Sn) and Pn attenuation in the Arabian Plate and surrounding regions, *Geophys. J. Int.*, *157*, 775–795, doi:10.1111/j.1365-246X.2004.02246.x.

Al-Lazki, A. I., D. Seber, E. Sandvol, N. Turkelli, R. Mohamad, and M. Barazangi (2003), Tomographic Pn velocity and anisotropy structure beneath the Anatolian plateau (eastern Turkey) and the surrounding regions, *Geophys. Res. Lett.*, *30*(24), 8043, doi:10.1029/2003GL017391.

Al-Lazki, A., E. Sandvol, D. Seber, M. Barazangi, N. Turkelli, and R. Mohamad (2004), Pn tomographic imaging of mantle

lid velocity and anisotropy at the junction of the Arabian, Eurasian and African plates, *Geophys. J. Int.*, *158*, 1024–1040, doi:10.1111/j.1365-246X.2004.02355.x.
An, M., and Y. Shi (2006), Lithosphere thickness of the Chinese continent, *Phys. Earth Planet. Inter.*, *159*, 257–266.
Angus, D., D. Wilson, E. Sandvol, and J. Ni (2006), Lithospheric structure of the Arabian and Eurasian collision zone in eastern Turkey from S-wave receiver functions, *Geophys. J. Int.*, *166*, 1335–1346, doi:10.1111/j.1365-246X.2006.03070.x.
Asudeh, I. (1982), Seismic structure of Iran from surface and body wave data, *Geophys. J. R. Astron. Soc.*, *71*, 715–730.
Bird, P. (1978), Finite element modeling of lithospheric deformation: The Zagros collision orogeny, *Tectonophysics*, *50*, 307–336.
Bormann, P., G. Grunthal, R. Kind, and H. Montag (1996), Upper mantle anisotropy beneath central Europe from SKS wave splitting: Effects of absolute plate motion and lithosphere-asthenosphere boundary topography?, *J. Geodyn.*, *22*, 11–32.
Camp, V., and M. Roobol (1989), The Arabian continental alkali basalt province: Part I. Evolution of Harrat Rahat, Kingdom of Saudi Arabia, *Geol. Soc. Am. Bull.*, *101*, 71–95.
Cara, M., and J. Lévêque (1987), Waveform inversion using secondary observables, *Geophys. Res. Lett.*, *14*, 1046–1049.
Christensen, N., and W. Mooney (1995), Seismic velocity structure and composition of the continental crust: A global view, *J. Geophys. Res.*, *100*, 9761–9788.
Debayle, E. (1999), Sv-wave azimuthal anisotropy in the Australian upper mantle: Preliminary results from automated Rayleigh waveform inversion, *Geophys. J. Int.*, *137*, 747–754.
Debayle, E., and B. Kennett (2000), The Australian continental upper mantle: Structure and deformation inferred from surface waves, *J. Geophys. Res.*, *105*, 25,423–25,450.
Debayle, E., and M. Sambridge (2004), Inversion of massive surface wave data sets: Model construction and resolution assessment, *J. Geophys. Res.*, *109*, B02316, doi:10.1029/2003JB002652.
Debayle, E., J.-J. Lévêque, and M. Cara (2001), Seismic evidence for a plume in the upper mantle beneath the northeastern Afro/Arabian continent, *Earth Planet. Sc. Lett.*, *193*, 423–436.
Dewey, F., J. M. Hempton, W. Kidd, F. Sarolu, and A. Şengör (1986), Shortening of the continental lithosphere: The neotectonics of eastern Anatolia—A young collision zone, in *Collision Tectonics*, edited by M. Conrad and A. Rise, *Geol. Soc. Spec. Publ.*, *19*, 2–36.
Dziewonski, M. A., and D. Anderson (1981), Preliminary Reference Earth Model, *Phys. Earth Planet. Inter.*, *25*, 297–356.
Engdahl, E., R. van der Hilst, and R. Bulland (1998), Global teleseismic earthquake relocation with improved travel times and procedures for depth determination, *Bull. Seismol. Soc. Am.*, *88*, 722–743.
Falcon, N. (1969), Problems of the relationship between surface structure and deep displacements illustrated by the Zagros Range, in *Time and Place in Orogeny*, edited by P. Kent, *Geol. Soc. Spec. Publ.*, *3*, 9–21, doi:10.1144/GSL.SP.1969.003.01.02.
Fouch, M., K. Fischer, E. Parmentier, M. Wysession, and T. Clarke (2000), Shear wave splitting, continental keels, and patterns of mantle flow, *J. Geophys. Res.*, *105*, 6255–6275.
Gelati, R. (1975), Miocene marine sequence from Lake Van, eastern Turkey, *Riv. Ital. Paleontol. Stratigr.*, *81*, 477–490.
Goes, S., R. Govers, and P. Vacher (2000), Shallow mantle temperatures under Europe from P and S wave tomography, *J. Geophys. Res.*, *105*, 11,153–11,169.
Gök, R., E. Sandvol, N. Türkelli, D. Seber, and M. Barazangi (2003), Sn attenuation in the Anatolian and Iranian plateau and surrounding regions, *Geophys. Res. Lett.*, *30*(24), 8042, doi:10.1029/2003GL018020.
Hafkenscheid, E., M. J. R. Wortel, and W. Spakman (2006), Subduction history of the Tethyan region derived from seismic tomography and tectonic reconstructions, *J. Geophys. Res.*, *111*, B08401, doi:10.1029/2005JB003791.
Hansen, S., S. Schwartz, A. Al-Amri, and A. Rodgers (2006), Combined plate motion and density-driven flow in the asthenosphere beneath Saudi Arabia: Evidence from shear-wave splitting and seismic anisotropy, *Geology*, *34*, 869–872, doi:10.1130/G22713.1.
Hansen, S., A. Rodgers, S. Schwartz, and A. Al-Amri (2007), Imaging ruptured lithosphere beneath the Red Sea and Arabian Peninsula, *Earth Planet. Sci. Lett.*, *259*, 256–265, doi:10.1016/j.epsl.2007.04.035.
Hatzfeld, D., and P. Molnar (2010), Comparisons of the kinematics and deep structures of the Zagros and Himalaya and of the Iranian and Tibetan plateaus and geodynamic implications, *Rev. Geophys.*, *48*, RG2005, doi:10.1029/2009RG000304.
Hatzfeld, D., M. Tatar, K. Priestley, and M. Ashtiany (2003), Seismological constraints on the crustal velocity structure beneath the Zagros Mountain belt (Iran), *Geophys. J. Int.*, *155*, 403–410.
Haynes, S. J., and H. McQuillan (1974), Evolution of the Zagros suture zone, southern Iran, *Geol. Soc. Am. Bull.*, *85*, 739–744.
Hearn, T., and J. Ni (1994), P_n velocities beneath continental collision zones: The Turkish-Iranian plateau, *Geophys. J. Int.*, *117*, 273–283.
Houseman, G., D. McKenzie, and P. Molnar (1981), Convective instability of a thickened boundary layer and its relevance for the thermal evolution of continental convergent belts, *J. Geophys. Res.*, *86*, 6115–6132.
Jackson, J. (1980), Errors in focal depth determination and the depth of seismicity in Iran and Turkey, *Geophys. J. R. Astron. Soc.*, *61*, 285–301.
Jackson, J., K. Priestley, M. Allen, and M. Berberian (2002), Active tectonics of the South Caspian Basin, *Geophys. J. Int.*, *148*, 214–245.
Jordan, T. (1975), The continental tectosphere, *Rev. Geophys.*, *13*, 1–12.
Kadinsky-Cade, K., M. Barazangi, J. Oliver, and B. Isacks (1981), Lateral variations in high-frequency seismic wave propagation at regional distances across the Turkish and Iranian plateaus, *J. Geophys. Res.*, *86*, 9377–9396.
Kaviani, A., A. Paul, E. Bourova, D. Hatzfeld, H. Pedersen, and M. Mokhtari (2007), A strong seismic velocity contrast in the shallow mantle across the Zagros collision zone (Iran), *Geophys. J. Int.*, *171*, 399–410, doi:10.1111/j.1365-246X.2007.03535.x.
Kaviani, A., D. Hatzfeld, A. Paul, M. Tatar, and K. Priestley (2009), Shear wave splitting, lithospheric anisotropy, and mantle deformation beneath the Arabia-Eurasia collision zone in Iran, *Earth Planet. Sci. Lett.*, *286*, 371–378, doi.org/10.1016/j.epsl.2009.07.003.
Kennett, B., and E. Enghdal (1991), Traveltimes for global earthquake location and phase identification, *Geophys. J. Int.*, *105*, 429–465.

Keskin, M. (2003), Magma generation by slab steepening and breakoff beneath a subduction-accretion complex: An alternative model for collision-related volcanism in Eastern Anatolia, Turkey, *Geophys. Res. Lett.*, *30*(24), 8046, doi:10.1029/2003GL018019.

Koop, W., and R. Stoneley (1982), Subsidence history of the Middle East Zagros basin, Permian to recent, *Philos. Trans. R. Soc. A*, *305*, 149–168.

Lei, J., and D. Zhao (2007), Teleseismic evidence for a breakoff subducting slab under eastern Turkey, *Earth Planet. Sci. Lett.*, *257*, 14–28.

Maggi, A., and K. Priestley (2005), Surface waveform tomography of the Turkish–Iranian Plateau, *Geophys. J. Int.*, *160*, 1068–1080.

Maggi, A., J. Jackson, D. McKenzie, and K. Priestley (2000a), Earthquake focal depths, effective elastic thickness, and the strength of the continental lithosphere, *Geology*, *28*, 495–498.

Maggi, A., J. Jackson, K. Priestley, and C. Baker (2000b), A re-assessment of focal depth distribution in southern Iran, the Tien Shan and northern India: Do earthquakes really occur in the continental mantle?, *Geophys. J. Int.*, *143*, 629–661.

Maggi, A., E. Debayle, K. Priestley, and G. Barruol (2006), Multimode surface waveform tomography of the Pacific Ocean: A closer look at the lithospheric cooling signature, *Geophys. J. Int.*, *166*, 1384–1397, doi:10.1111/j.1365-24X.2006.03037.x.

Martinez, F., and J. Cochran (1988), Structure and tectonics of the northern Red Sea: Catching a continental margin between rifting and drifting, *Tectonophysics*, *150*, 1–32.

McClusky, S., R. Reilinger, S. Mahmoud, D. Ben Sari, and A. Tealeb (2003), GPS constraints on Africa (Nubia) and Arabia plate motions, *Geophys. J. Int.*, *155*, 126–138.

McKenzie, D., and K. Priestley (2008), The influence of lithospheric thickness variations on continental evolution, *Lithos*, *102*, 1–11, doi:10.1016/j.lithos.2007.05.005.

McKenzie, D., J. Jackson, and K. Priestley (2005), Thermal structure of oceanic and continental lithosphere, *Earth Planet. Sc. Lett.*, *233*, 337–349.

McQuarrie, N. (2004), Crustal-scale geometry of the Zagros fold-and-thrust belt, Iran, *J. Struct. Geol.*, *26*, 519–535.

McQuarrie, N., J. M. Stock, C. Verdel, and B. P. Wernicke (2003), Cenozoic evolution of Neotethys and implications for the causes of plate motions, *Geophys. Res. Lett.*, *30*(20), 2036, doi:10.1029/2003GL017992.

Molinaro, M., H. Zeyen, and X. Laurencin (2005), Lithospheric structure beneath the south-eastern Zagros Mountains, Iran: Recent slab break-off?, *Terra Nova*, *17*, 1–6, doi:10.1111/j.1365-3121.2004.00575.x.

Molnar, P., and H. Lyon-Caen (1988), Some physical aspects of the support, structure and evolution of mountain belts, in *Processes in Continental and Lithospheric Deformation*, edited by J. Clark, *Spec. Pap. Geol. Soc. Am.*, *218*, 179–207.

Molnar, P., and J. Oliver (1969), Lateral variations of attenuation in the uppermost mantle and discontinuities in the lithosphere, *J. Geophys. Res.*, *74*, 2648–2683.

Montagner, J. (1986), Regional three-dimensional structures using long-period surface waves, *Ann. Geophys.*, *4*, 283–294.

Motaghi, K., M. Tatar, and K. Priestley (2011), Crustal thickness variations across the northeast Iran continental collision zone from teleseismic converted waves, *J. Seismol.*, *16*, 253–260, doi:10.1007/s10950-011-9267-2.

Motaghi, K., M. Tatar, Z. Shomali, A. Kaviana, and K. Priestley (2012), High resolution image of uppermost mantle beneath NE Iran continental collision zone, *Phys. Earth Planet. Inter.*, *208–209*, 38–49.

Ni, J., and M. Barazangi (1986), Seismotectonics of Zagros continental collision zone and a comparison with the Himalayas, *J. Geophys. Res.*, *91*, 8205–8218.

Nowrouzi, G., K. Priestley, M. Ghafory-Ashtiany, G. Doloei, and D. Rham (2007), Crustal velocity structure in Iranian Kopeh-Dagh, from analysis of P-waveform receiver functions, *J. Seismol. Earthquake Eng.*, *8*, 187–194.

Omrania, J., P. Agarda, H. Whitechurch, M. Benoit, G. Prouteau, and L. Jolivet (2008), Arc-magmatism and subduction history beneath the Zagros Mountains, Iran: A new report of adakites and geodynamic consequences, *Lithos*, *106*, 380–398, doi:10.1016/j.lithos.2008.09.008.

Park, Y., A. A. Nyblade, A. J. Rodgers, and A. Al-Amri (2008), S wave velocity structure of the Arabian Shield upper mantle from Rayleigh wave tomography, *Geochem. Geophys. Geosyst.*, *9*, Q07020, doi:10.1029/2007GC001895.

Paul, A., A. Kaviani, D. Hatzfeld, J. Vergne, and M. Mokhtari (2006), Seismological evidence for crustal-scale thrusting in the Zagros mountain belt (Iran), *Geophys. J. Int.*, *166*, 227–237.

Pearce, J., et al. (1990), Genesis of collision volcanism in eastern Anatolia, Turkey, *J. Volcanol. Geotherm. Res.*, *44*, 189–229.

Priestley, K., and D. McKenzie (2006), The thermal structure of the lithosphere from shear wave velocities, *Earth Planet. Sc. Lett.*, *244*, 285–301.

Priestley, K., C. Baker, and J. Jackson (1994), Implications of earthquake focal mechanism data for the active tectonics of the south Caspian Basin and surrounding regions, *Geophys. J. Int.*, *118*, 111–141.

Priestley, K., E. Debayle, D. McKenzie, and S. Pilidou (2006), Upper mantle structure of eastern Asia from multimode surface waveform tomography, *J. Geophys. Res.*, *111*, B10304, doi:10.1029/2005JB004082.

Reilinger, R., et al. (2006), GPS constraints on continental deformation in the Africa-Arabia-Eurasia continental collision zone and implications for the dynamics of plate interactions, *J. Geophys. Res.*, *111*, B05411, doi:10.1029/2005JB004051.

Rham, D. (2009), The crustal structure of the Middle East, PhD thesis, Univ. of Cambridge, Cambridge, U. K.

Robertson, A. (2000), Mesozoic-Tertiary tectonic-sedimentary evolution of a south Tethyan oceanic basin and its margins in southern Turkey, in *Tectonics and Magmatism in Turkey and the Surounding Area*, edited by E. Bozkurt, J. Winchester, and J. Piper, *Geol. Soc. Spec. Publ.*, *173*, 97–138.

Rodgers, A., J. Ni, and T. Hearn (1997), Propagation characteristics of short-period S_n and L_g in the Middle East, *Bull. Seismol. Soc. Am.*, *87*, 396–413.

Rodgers, A., W. Walter, R. Mellors, A. Al-Amri, and Y.-S. Zhang (1999), Lithospheric structure of the Arabian Shield and Platform from complete regional waveform modelling and surface wave group velocities, *Geophys. J. Int.*, *138*, 871–878.

Sandvol, E., K. Al-Damegh, A. Calvert, D. Seber, M. Barazangi, R. Mohamad, R. Gok, N. Turkelli, and C. Gurbuz (2001), Tomographic imaging of L_g and S_n propagation in the Middle East, *Pure Appl. Geophys.*, *158*, 1121–1163.

Sandvol, E., N. Turkelli, E. Zor, R. Gok, T. Bekler, C. Gurbuz, D. Seber, and M. Barazangi (2003), Shear wave splitting in a young continent-continent collision: An example from eastern Turkey, *Geophys. Res. Lett.*, *30*(24), 8041, doi:10.1029/2003GL017390.

Sattarzadeh, Y., J. Cosgrove, and C. Vita-Finzi (1999), The interplay of faulting and folding during the evolution of the Zagros deformation belt, *Geol. Soc. Spec. Publ.*, *169*, 187–196, doi:10.1144/GSL.SP.2000.169.01.14.

Sen, P., A. Temel, and A. Gourgaund (2004), Petrogenetic modelling of Quaternary post-collisional volcanism: A case study of central and eastern Anatolia, *Geol. Mag.*, *141*, 81–98.

Şengör, A. (1990), A new model for the late Paleozoic-Mesozoic tectonic evolution of Iran and implications for Oman, in *The Geology and Tectonics of the Oman Region*, edited by A. Robertson, M. Searle, and A. Ries, *Geol. Soc. Spec. Publ.*, *49*, 797–831.

Şengör, A., and W. Kidd (1979), Post-collisional tectonics of the Turkish–Iranian Plateau and a comparison with Tibet, *Tectonophysics*, *55*, 361–376.

Şengör, A., S. Ozeren, T. Genc, and E. Zor (2003), East Anatolian high plateau as a mantle-supported, north-south shortened domal structure, *Geophys. Res. Lett.*, *30*(24), 8045, doi:10.1029/2003GL017858.

Şengör, A., S. Ozeren, M. Keskin, M. Sakinc, A. Ozbakir, and I. Kayan (2008), Eastern Turkish high plateau as a small Turkic-type orogen: Implications for post-collisional crust-forming process in Turkic-type orogens, *Earth Sci. Rev.*, *90*, 1–48.

Shapiro, N., M. Ritzwoller, J. Mareschal, and C. Jaupart (2004), Lithospheric structure of the Canadian shield inferred from inversion of surface-wave dispersion with thermodynamic a priori constraints, in *Geological Prior Information*, edited by A. Curtis and R. Wood, *Geol. Soc. Spec. Publ.*, *239*, 175–194.

Shaw, J., J. Baker, M. Menzies, M. Thirlwall, and K. Ibrahim (2003), Petrogenesis of the largest intraplate volcanic field on the Arabian Plate (Jordan): A mixed lithosphere: Asthenosphere source activated by lithospheric extension, *J. Petrol.*, *44*, 1657–1679.

Silver, P. G. (1996), Seismic anisotropy beneath the continents, probing the depths of geology, *Annu. Rev. Earth Planet. Sci.*, *24*, 385–432.

Snyder, D., and M. Barazangi (1986), Deep crustal structure and flexure of the Arabian plate beneath the Zagros collisional mountain belt as inferred from gravity observations, *Tectonics*, *5*, 361–373.

Stocklin, J. (1968), Structural history and tectonics of Iran: A review, *Am. Assoc. Pet. Geol. Bull.*, *52*, 1229–1258.

Stocklin, J., and M. Naloavi (1971), Tectonic map of Iran, scale 1:2,500,00, Geol. Surv. of Iran, Tehran.

Talebian, M., and J. Jackson (2004), A reapprasial of earthquake focal mechanisms and active faulting and active shortening in the Zagros Mountains of Iran, *Geophys. J. Int.*, *156*, 506–526.

Tatar, M., D. Hatzfeld, J. Martinod, A. Walpersdorf, M. Ghafori-Ashtiany, and J. Chéry (2002), The present-day deformation of the central Zagros from GPS measurements, *Geophys. Res. Lett.*, *29*(19), 1927, doi:10.1029/2002GL015427.

Tatar, M., D. Hatzfeld, and M. Ghafori-Ashtiany (2004), Tectonics of the Central Zagros (Iran) deduced from microearthquake seismicity, *Geophys. J. Int.*, *156*, 255–266.

Tatar, M., J. Jackson, D. Hatzfeld, and E. Bergman (2007), The 2004 May 28 Baladeh earthquake (M_w 6.2) in the Alborz, Iran: Overthrusting the South Caspian Basin margin, partitioning of oblique convergence and the seismic hazard of Tehran, *Geophys. J. Int.*, *170*, 249–261.

Tkalčić, H., M. Pasyanos, A. Rodgers, R. Gök, W. Walter, and A. Al-Amri (2006), A multistep approach for joint modeling of surface wave dispersion and teleseismic receiver functions: Implications for lithospheric structure of the Arabian Peninsula, *J. Geophys. Res.*, *111*, B11311, doi:10.1029/2005JB004130.

Turkelli, N., et al. (2003), Seismogenic zones in eastern Turkey, *Geophys. Res. Lett.*, *30*(24), 8039, doi:10.1029/2003GL018023.

VanDecar, J., and R. Crosson (1990), Determination of teleseismic relative phase arrival times using multi-channel cross-correlation and least squares, *Bull. Seismol. Soc. Am.*, *80*, 150–169.

Vernant, P., et al. (2004), Present-day crustal deformation and plate kinematics in Middle East constrained by GPS measurements in Iran and northern Oman, *Geophys. J. Int.*, *157*, 381–398.

Walker, R., P. Gans, M. Allan, J. Jackson, M. Khatib, A. Saunders, and M. Zarrinkoub (2009), Late Cenozoic volcanism and rates of active faulting in eastern Iran, *Geophys. J. Int.*, *177*, 783–805, doi:10.1111/j.1365-246X.2008.04024.x.

Wells, A. (1969), The crush zone of the Iranian Zagros Mountains, and its implications, *Geol. Mag.*, *106*, 385–394, doi:10.1017/S0016756800058787.

Wessel, P., and W. Smith (1995), New version of the Generic Mapping Tool release, *Eos Trans. AGU*, *76*, 329.

White, R., D. McKenzie, and R. O'Nions (1992), Oceanic crustal thickness from seismic measurements and rare earth element inversions, *J. Geophys. Res.*, *97*, 19,683–19,715.

Zor, E. (2008), Tomographic evidence of slab detachment beneath eastern Turkey and the Caucasus, *Geophys. J. Int.*, *175*, 1273–1282, 2008, doi:10.1111/j.1365-246X.2008.03946.x.